Granular materials under vibration: Simulations of rotating spheres

S. Luding
Theoretische Polymerphysik, Rheinstrasse 12, D-79104 Freiburg, Germany
and Laboratoire d'Accoustique et d'Optique de la Matière Condensée, URA 800, Université Pierre et Marie Curie, 4 place Jussieu, 75005 Paris, France
(Received 30 March 1995)

We present simulations of spheres with a rough surface in two-dimensional (2D) vibrating boxes. We introduce a collision model based on recent experiments with colliding spheres. During the collision of two rough particles energy is dissipated and, possibly, linear momentum is transferred to rotational momentum. We examine the model system by varying the parameters, as for example the coefficient of friction, μ. Using an event driven algorithm, we focus on the fluidized regime, i.e., on the case of rather small densities. We find that the behavior of the system depends on the frictional properties of both particles and walls. Introducing particle-particle friction changes the behavior quantitatively. Rough, dissipative walls lead to a qualitative change of the system's behavior in the case of low densities. We present an expression for the ratio of kinetic and rotational energy in terms of the particles' moment of inertia, of the coefficient of friction, and of the tangential restitution. Furthermore, we compare our simulations with recent experiments on vibrated granular systems in 2D.

PACS number(s): 46.10.+z, 05.60.+w, 05.40.+j

I. INTRODUCTION

The behavior of dry granular materials is important for various applications, such as transport, storage, or mixing. In recent years a lot of effort has been invested in the understanding of effects such as size segregation [1–4], heap-formation [5,6], and convection [7–9]. Also phenomena like surface waves [10,11], sound wave propagation [12,13], and the so-called "decompaction" [14] were recently examined. For a review see Ref. [15]. In this study we focus on granular model media in 2D under vertical vibrations in the gravitational field. Also this system recently received a lot of interest [16–22].

Due to the complex dynamics and the dissipative nature of granular systems, analytical approaches, i.e., kinetic theories [23–25], are quite difficult to handle and can be solved only in small ranges of parameter space. Mazighi *et al.* [20] solved the dissipative Boltzmann equation, for a one-dimensional (1D) system, in the limits of weak and strong dissipation. Detailed experimental studies of granular systems are necessary in order to aid the progress in theoretical research.

The experimental assessment of local quantities, such as granular temperature or pressure, is extremely difficult. However, an experimental setup was developed that uses digital high-speed photography to track the linear and angular motion of the particles [16,21,26] in 2D systems.

In addition, numerical simulations are an adequate tool to study the behavior of dissipative granulates and thus complement experiments and theories. The majority of granular media simulations are performed using molecular dynamics (MD) methods [8,9,27–30], but also event driven (ED) algorithms [18–20,31–34] are used. For a comparison of both methods see [19,28,31,35]. MD algorithms, in general, integrate Newton's equations of motion at fixed intervals of time. ED algorithms, in contrast, evaluate the time of the next contact and compute the particles' velocities after this event. Both simulation methods are based on assumptions about the interaction of the particles. In MD simulations contact forces are active as long as particles overlap, whereas in ED simulations the particles do not overlap and the contact is assumed to be instantaneous.

Recently, vibrated granular media were examined numerically and experimentally in 1D [17,18,20] and also in 2D [19,36,37]. The transition from a fluidized to a condensed regime was observed and scaling laws for the different parameters were found. In the fluidized regime the reduced height of the center of mass, H, scales with the typical velocity of the vibrating container, V. The behavior of H follows the law $H \propto V^{\delta}$ and both simulations and experiments lead to $\delta = 2$ in 1D, and $\delta < 2$ in 2D. The astonishing and theoretically unexpected finding is that the power is smaller than 2 in 2D. Luding *et al.* [19] observed a power $\delta = 1.5$, whereas Warr *et al.* [16] found values between $\delta = 1.3$ and $\delta = 1.4$ [16]. In contrast, kinetic theory approaches [16,22] lead to the power $\delta = 2$. Besides the V scaling, both experiment and simulations predict that H decreases with an increasing number of particles N, i.e., $H \propto N^{-\nu}$. Numerical simulations show $\nu = 1$ [19], whereas experiments lead to the power $0.3 < \nu < 1$ [16]. Thus, the experimental results show that the simplified numerical model without rotation [19] overestimates the exponents δ and ν. Our aim is now to allow rotation in the numerical model of Ref. [19] and to examine the behavior of the system in this case. Furthermore, we will compare the numerical results with the experimental data of Ref. [16].

In Sec. II we describe the collision model and intro-

duce the new parameters necessary to handle rotating particles. The numerical method and the boundary conditions are presented in Sec. III. Section IV contains several examples of binary collisions while in Sec. V the simulational results are discussed. Finally, we summarize and conclude in Sec. VI.

II. THE COLLISION MODEL

Our description of the collisions of particles are based on the ideas of Maw, Barber, and Fawcett [38] and therefore, we apply the simplified collision model introduced by Walton *et al.* [29] and recently established experimentally by Foerster *et al.* [26].

For given velocities before contact, we need three coefficients to evaluate the velocities after the collision. The first, the coefficient of normal restitution, ϵ, defines the incomplete restitution of the normal component of the relative velocity. The second, the coefficient of friction, μ, relates the tangential force to the normal force, i.e., Coulomb's law. The third, the coefficient of maximum tangential restitution, β_0, limits the restitution of tangential velocity of the contact point, when contacts are broken. Note that this model implies that a contact either follows Coulomb's law or breaks [26,29]. In the following, we apply the basic conservation laws and determine the equations for the velocities after one collision.

Consider two particles with diameters d_1 and d_2 and masses m_1 and m_2. The normal unit vector for their contact is

$$\vec{n} = \frac{\vec{r}_1 - \vec{r}_2}{|\vec{r}_1 - \vec{r}_2|}, \tag{1}$$

where $\vec{r}_i$ is the vector to the center of particle i ($i = 1, 2$). The relative velocity of the contact point is

$$\vec{v}_c = \vec{v}_1 - \vec{v}_2 - \left(\frac{d_1}{2}\vec{\omega}_1 + \frac{d_2}{2}\vec{\omega}_2\right) \times \vec{n}, \tag{2}$$

where $\vec{v}_i$ and $\vec{\omega}_i$ are the linear and angular velocities before collision of particle i. We remark that $v_c = |\vec{v}_c|$ increases when, for example, the particle velocities point to opposite directions and the angular velocities point to the same direction. $\vec{v}_c$ has the normal component $\vec{v}_c^{(n)} = \vec{n}(\vec{v}_c \cdot \vec{n})$ and the tangential component $\vec{v}_c^{(t)} = \vec{v}_c - \vec{v}_c^{(n)}$. The vector $\vec{v}_c^{(t)}$ defines the direction of the tangential unit vector $\vec{t} = \vec{v}_c^{(t)}/|\vec{v}_c^{(t)}|$. The impact angle, γ, is defined as the angle between $\vec{n}$ and $\vec{v}_c$ and we always have $\pi/2 < \gamma \leq \pi$. For illustration, we give a schematic picture of two colliding particles, with $\omega_1 = \omega_2 = 0$, just before a collision in Fig. 1(a).

The momentum conservation law leads to the change of linear momentum of particle 1,

$$\Delta\vec{P} = m_1(\vec{u}_1 - \vec{v}_1) = -m_2(\vec{u}_2 - \vec{v}_2), \tag{3}$$

with $\vec{u}_i$ designating the unknown velocity of particle i after the collision. The normal component, $\Delta\vec{P}^{(n)}$, does not affect the angular velocities, whereas the tangential

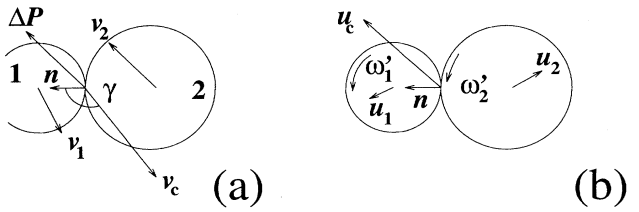

FIG. 1. Typical velocities of two particles just before (a) and just after (b) collision.

component $\Delta\vec{P}^{(t)}$ leads to a change of angular momentum. $\Delta\vec{P}^{(t)}$ is active at the contact point, perpendicular to the momentarm, $-(d_1/2)\vec{n}$. Therefore, the vector product of the moment arm and $\Delta\vec{P}$ leads to the change of angular momentum

$$-\vec{n} \times \Delta\vec{P} = \frac{2I}{d}(\vec{\omega}' - \vec{\omega}). \tag{4}$$

In Eq. (4) I is the moment of inertia about the center of a particle and $\vec{\omega}'$ is the unknown angular velocity after contact. Note that Eq. (4) leads to the same change of angular momentum for both particles. We plot the velocities after contact schematically in Fig. 1(b).

From $\Delta\vec{P}$ we get the velocities after the collision from Eqs. (3) and (4):

$$\vec{u}_1 = \vec{v}_1 + \Delta\vec{P}/m_1, \tag{5a}$$

$$\vec{\omega}_1' = \vec{\omega}_1 - \frac{d_1}{(2I_1)}\vec{n} \times \Delta\vec{P}, \tag{5b}$$

$$\vec{u}_2 = \vec{v}_2 - \Delta\vec{P}/m_2, \tag{5c}$$

$$\vec{\omega}_2' = \vec{\omega}_2 - \frac{d_2}{(2I_2)}\vec{n} \times \Delta\vec{P}. \tag{5d}$$

At first, we calculate the normal component of the momentum change, $\Delta\vec{P}^{(n)}$, using the definition of the coefficient of normal restitution

$$\vec{u}_c^{(n)} = -\epsilon\vec{v}_c^{(n)}, \tag{6}$$

that connects the normal velocity after contact, $\vec{u}_c^{(n)}$, with the normal velocity before contact, for $0 \leq \epsilon \leq 1$. Here, nothing is said about a possible velocity dependence of ϵ [28].

Inserting Eq. (6) into the normal component of the sum $\Delta\vec{P}/m_1 + \Delta\vec{P}/m_2$, see Eq. (3), we get the normal component of the momentum change

$$\Delta\vec{P}^{(n)} = -m_{12}(1+\epsilon)\vec{v}_c^{(n)}, \tag{7}$$

with the reduced mass $m_{12} = m_1 m_2/(m_1 + m_2)$.

Coulomb's law relates the tangential and the normal

components of $\Delta\vec{P}$, i.e., $|\Delta\vec{P}^{(t)}| = \mu|\Delta\vec{P}^{(n)}|$, with the coefficient of friction, $\mu \geq 0$. Since the contact is dissipative, the direction of $\Delta\vec{P}^{(t)}$ is opposite to $\vec{v}_c^{(t)}$ and thus given by $-\vec{t}$. Therefore, the tangential component of the change of momentum is

$$\Delta\vec{P}^{(t)} = \mu m_{12}(1+\epsilon)v_c \cos\gamma\ \vec{t}\,, \tag{8}$$

with $v_c^{(n)} = |\vec{v}_c^{(n)}| = -v_c\cos\gamma$, because $\cos\gamma \leq 0$ for all possible γ. Together with the definition of $\vec{t} = \vec{v}_c^{(t)}/(v_c\sin\gamma)$, the sum of Eqs. (7) and (8) leads to the change of momentum

$$\Delta\vec{P} = -m_{12}(1+\epsilon)\vec{v}_c^{(n)} + m_{12}\mu(1+\epsilon)\cot\gamma\ \vec{v}_c^{(t)}, \tag{9}$$

see also Eq. (7) in Ref. [26]. Note that $\cot\gamma \to -\infty$ for $\gamma \to \pi$, where $\gamma = \pi$ is the limit of a central collision. In this limit of small tangential velocities $\Delta P^{(t)}$ may get very large and thus $|\vec{u}^{(t)}|$ may get greater than $|\vec{v}^{(t)}|$ if one simply inserts Eq. (9) in Eqs. (5a) and (5c). This would lead to an increase of energy and thus limits Eq. (9) and thereby Coulomb's law to rather small impact angles, i.e., large tangential velocities. The case of large $\Delta P^{(t)}$ corresponds to a large force in the tangential direction, acting during contact. Such a large force eventually breaks the contact and leads to a nonfrictional tangential motion of the two surfaces. In order to handle this case, Walton *et al.* [29] and Foerster *et al.* [26] introduce the coefficient of maximum tangential restitution β_0 with $-1 \leq \beta_0 \leq 1$ [39], which limits the tangential restitution in the case of broken contacts, i.e., large γ or small tangential velocities.

We rewrite Eq. (9) to get a form that contains the coefficient of normal restitution and the tangential restitution, β, in a similar manner. The tangential restitution is defined by the tangential equivalent to Eq. (6), i.e., $\vec{u}_c^{(t)} = -\beta\vec{v}_c^{(t)}$, and, in general, depends on γ. Thus, the momentum change is

$$\Delta\vec{P} = -m_{12}(1+\epsilon)\vec{v}_c^{(n)} - \tfrac{2}{7}m_{12}(1+\beta)\vec{v}_c^{(t)} \tag{10}$$

for solid spheres. The factor 2/7 stems from the fact that a change of linear tangential velocity is always connected to a change of angular momentum and depends on the moment of inertia of the involved particles. In Eq. (10) we have $\beta = \min[\beta_0, \beta_1]$. For large γ and thus broken contacts, we use $\beta = \beta_0$. Inserting $\beta = \beta_1 = -1 - \frac{7}{2}\mu(1+\epsilon)\cot\gamma$ in Eq. (10) leads to Eq. (9) and corresponds to Coulomb-type contacts for small γ. For a detailed calculation of β_1 see Appendix A.

We plot β as a function of γ in Fig. 2(a). Negative β values lead to a decrease of $v_c^{(t)}$ during contact, whereas positive β values correspond to an inversion of the direction of $\vec{v}_c$. $|\beta| < 1$ means that the absolute value of the relative velocity is smaller after the collision than before. This somewhat simplified model allows only Coulomb friction, for $\gamma < \gamma_0$, or only broken contacts, for $\gamma \geq \gamma_0$, whereas in nature both kinds of contact might coexist [38]. The angle γ_0 follows from $\beta_0 = \beta_1$, i.e., $-\tan\gamma_0 = (7/2)\mu(1+\epsilon)/(1+\beta_0)$.

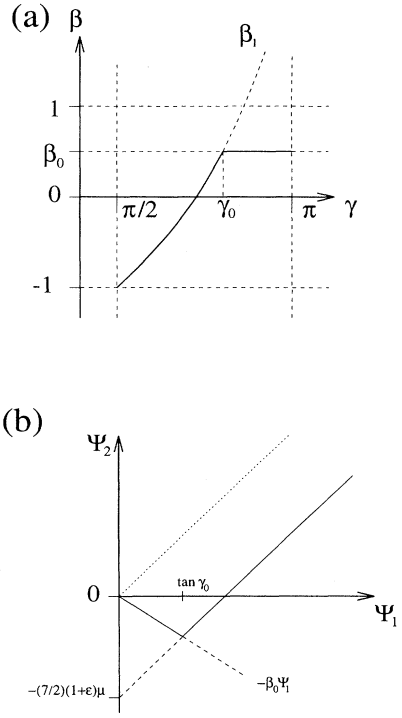

FIG. 2. (a) Schematic plot of the tangential restitution β as a function of the impact angle γ. (b) Schematic picture of $\Psi_2 = u_c^{(t)}/v_c^{(n)}$ as a function of $\Psi_1 = v_c^{(t)}/v_c^{(n)}$.

In order to classify quantitatively the collisions, Foerster *et al.* [26] use the ratios of tangential and normal velocities. We define $\Psi_1 = v_c^{(t)}/v_c^{(n)} = -\tan\gamma$ and $\Psi_2 = u_c^{(t)}/v_c^{(n)} = \epsilon\tan\gamma'$, where γ' is the angle between $\vec{u}_c$ and $\vec{n}$. This leads to

$$\Psi_2 = \Psi_1 - \tfrac{7}{2}(1+\epsilon)\mu \tag{11}$$

for Coulomb contacts and to

$$\Psi_2 = -\beta_0\Psi_1 \tag{12}$$

for broken contacts. Coulomb-type contacts occur for large Ψ_1, i.e., $\gamma < \gamma_0$, and broken contacts for small Ψ_1, i.e., $\gamma \geq \gamma_0$. We plot a schematic picture of Ψ_2 as a function of Ψ_1 in Fig. 2(b). The dotted line shows the case of $\mu = 0$, i.e., no friction, and the solid line follows Eqs. (11) and (12) in their ranges of validity. For a given set of parameters, ϵ, μ, and β_0, each possible collision will correspond to one point on the solid line in Fig. 2(b).

From Eq. (10) we calculate the ratio of tangential and normal momentum change as a function of γ in Appendix B. This ratio is connected to the ratio of the integrals over tangential and normal forces and is one possible presentation of Coulomb's law.

III. THE SIMULATION METHOD

Granular materials consist of mesoscopic particles, whose surface is rough at least on a microscopic scale. Usually, one models granulates by spheres, with either a perfectly smooth or a rough surface. Recent publications [30], using nonspherical particles, also take into account the asymmetric nature of, e.g., real sand. However, the consequence of a rough surface is solid friction: If two particles touch each other, a finite force F_s is needed to trigger tangential motion and if two particles move against each other, a finite force F_d is needed to maintain the motion. Solid friction leads to a change of linear and angular momentum as well. Therefore, a rough surface implies both rotation and energy loss. Thus, it is important to allow rotation as soon as particles are assumed to have a rough surface. In simulations, we describe the roughness of surfaces and the connected energy dissipation, using the parameters μ and β_0, as introduced in Sec. II.

Further mechanisms of energy loss are, for example, the permanent deformation of a particle during contact, or the transfer of kinetic energy to thermal energy, i.e. vibrational energy. We account for those effects, using the coefficient of normal restitution, ϵ.

A. Event driven simulations

Our model system is a rectangular container of width L, open at the top. The vertical position of the bottom of the box at time t is

$$z_0(t) = A_0 \sin(2\pi f t), \tag{13}$$

where f is the frequency and A_0 is the amplitude. The typical velocity of the motion is $V = A_0\omega$, with $\omega = 2\pi f$. The container is filled with N spherical particles with diameter d_i ($i = 1, ..., N$). If not explicitly mentioned, we have d_i uniformly distributed in the range $d_0 - w_0 \leq d_i \leq d_0 + w_0$, where $d_0 = 1$ mm and $w_0 = 0.1$ mm.

Since we are interested in the behavior of granular particles in the fluidized regime, where the density is rather small, we use an event driven (ED) method. In our simulations, the particles follow an undisturbed Newtonian motion, under the influence of gravity, until an event occurs. An event is either the collision of two particles or the collision of one particle with a wall. Using the velocities just before contact we compute the particles' velocities after the contact following Eqs. (5). Note that in the ED method the time for which two particles are in contact is implicitly zero. The consequence is that exclusively two particle contacts occur. The assumption of pairwise contacts is reasonable for our system, since the time between contacts is, on average, much larger than the duration of a contact. The contact time of two steel spheres of diameter $d = 1$ mm is $t_c \approx 3 \times 10^{-6}$ s [28], whereas the time between events is of the order of $t_{ev} = 10^{-3}$ s, assuming an average separation of 0.1 mm and an average velocity of 0.1 m/s. In a recent publication it was proven that the results of ED simulations, with zero contact time, and of MD simulations, with a contact time greater than zero, agree well in the fluidized regime [19]. We remark that ED algorithms run into problems when t_{ev} gets to be small. In dense systems with strong dissipation t_{ev} may vanish and clusters will occur. A cluster is an array of particles in contact with zero relative energy. This problem, called inelastic collapse [20,33], may be handled, at least in 1D, using the largest relative velocity (LRV) procedure [18].

In recent papers a simple ED algorithm was used to simulate the behavior of 1D systems [17,18,20,28,33,35]. Such simple ED algorithms update the whole system after each event, a method which is straightforward, but inefficient for large numbers of particles. In Ref. [32] an ED algorithm was introduced which updates only those particles which were involved in the previous collision. For this a double buffering data structure is implemented, which contains the "old" status and the "new" status, each consisting of time of event, position, velocities, and partner. The "old" status of particle i has to be kept in memory, in order to calculate the time of the next contact, t_{ij}, of particle i with any other object j. An object j is either a particle ($j = 1, ..., i-1, i+1, ..., N$) or a wall ($j = N+1, N+2, N+3$). The minimum of all t_{ij} is stored in the "new" status of particle i, together with the corresponding partner j, but the velocities after the collision are not yet calculated. This would be a waste of computer time, since before the time t_{ij} the predicted partners i and j might be involved into several collisions with other particles. The minimum times of event, i.e., the times which indicate the next event for a certain particle, are stored in an ordered heap tree, such that the next event is found at the top of the heap. For a detailed description of the algorithm see Ref. [32].

As in Ref. [19,35] we implement the algorithm of Ref. [32] with some changes and further extensions. First, we introduce the gravitational force and the sinusoidally moving bottom. Despite the gravitational acceleration, all contact times of particles with each other or with the lateral walls can be calculated analytically. Unfortunately, the time of contact of any particle with the bottom of the box has to be computed numerically [18,19,35]. Second, we introduce dissipation, i.e., the normal velocity after contact is determined by the coefficient of normal restitution, ϵ. As an extension of the algorithm used in Ref. [19] we allow the particles to rotate and take care of solid friction by introducing the coefficient of friction, μ, and the coefficient of maximum tangential restitution, β_0. If, for example, the coefficient of normal restitution depends on the partner of the colliding particle, we use ϵ, ϵ_w, and ϵ_b for particle-particle, particle-wall, and particle-bottom collisions, respectively. The collision model is described in detail in Sec. II.

B. Boundary conditions

We are interested in the steady-state situation, where the average quantities of the system, like the height of the

center of mass, the kinetic energy, or the rotational energy, are constant. Using different initial conditions, we found no dependence of the steady state on the choice of either, different initial separation or different initial velocities. For each simulation run we trace the average quantities of the system at phase zero, i.e., the bottom moves upwards. We check that the steady state is reached, and perform the averages over a time larger than the time scale of typical fluctuations. We assume that the steady state is reached when the average quantities do not depend on the time intervals used for the averages. If the time of average is too small, the natural fluctuations of the averaged quantities get visible.

We use two configurations of the box. First, we fix the side walls and move only the bottom plate, and second, we move the whole container. If not explicitly mentioned the first configuration is used. As expected, we observe no differences between these configurations in the case of smooth sidewalls. The simulations were carried out on HP Apollo and IBM RS6000 Workstations.

IV. SOME EXAMPLES OF SIMPLE COLLISIONS

In order to get a qualitative idea concerning the importance of the parameters of tangential friction, i.e., μ and β_0, we first present some simulations of particle-wall and of particle-particle collisions. Therefore, we subsequently vary the initial tangential velocities μ, ϵ, and β_0, and we plot some snapshots at different times before and after collision.

A. Particle-wall collisions

To examine the influence of the coefficient of friction, μ_w, on collisions of particles with the walls, we perform several simulations, where we vary the tangential velocity, $v_0^{(t)}$, and the coefficient of friction, μ_w, while the normal velocity, $v_0^{(n)}$, and the coefficient of restitution, ϵ_w, stay constant. Our choice of the tangential velocities corresponds to certain values of Ψ_1, and thus, the value of Ψ_2 is also defined for each collision, see Sec. II. It is obvious that the tangential relative momentum is also partly transferred into rotational momentum. Only for $\mu_w = 0$, i.e., a perfectly smooth surface, no change of angular velocity will occur.

Snapshots from three simulations of eight pairs of particles colliding with the sidewalls are plotted in Fig. 3. We display four pictures of each simulation and the time between two pictures is 6 ms. The initial normal velocity is $v_0^{(n)} = 0.5$ m/s, relative to the sidewall, and the initial tangential velocities are from bottom to top $v_0^{(t)} = 0.0, 0.25,..., 1.75$ m/s, indicated by the lines. Our choice of the tangential velocity corresponds to the Ψ_1 values $\Psi_1 = 0, 0.5,...,$ and 3.5. The angular velocity initially equals zero and is indicated by the greyscale of the quarter circles, i.e., black corresponds to $\omega' = 0$ and white corresponds to $\omega' \geq 720$ rad/s. The actual angle of each particle is indicated by the position of the quarter circles. The coefficient of friction is set to $\mu_w = 0.2$ (a)–(d), $\mu_w = 0.5$ (e)–(h), and $\mu_w = 10^4$ (i)–(l), i.e., a completely rough surface. The coefficient of normal restitution is $\epsilon_w = 0.9$ and the coefficient of maximum tangential restitution is $\beta_{0w} = 0.5$.

In general, large tangential velocity, $v_0^{(t)}$, will lead to large angular velocity, ω', of the particle after the collision. However, the magnitude of ω' is limited by Coulomb's law and thus by μ_w. If the normal momentum change is rather small, the momentum transferred from linear to angular direction is small as well. With increasing tangential velocity the particles reach a maximum angular velocity, the value of which increases with increasing μ_w [compare Fig. 3(d) where $\mu_w = 0.2$ and Fig. 3(h) where $\mu_w = 0.5$]. For very large μ_w, i.e., a completely rough surface [Fig. 3(l)], the maximum angular velocity is not limited by the change of normal momentum.

To understand the influence of β_{0w} on the collisions of particles with walls, we perform further simulations with the same initial conditions as before for Fig. 3. We fix $\mu_w = 0.5$ and vary the coefficient of tangential restitution $\beta_{0w} = -0.5$, 0.0, and 0.5 for Figs. 4(a)–4(d), 4(e)–4(h), and 4(i)–4(l), respectively. These β_{0w} values correspond to $-\tan\gamma_0 = 6.65$, 3.33, and 2.22, such that $\Psi_1 < -\tan\gamma_0$, i.e., we have broken contacts, for all collisions, except the three uppermost in Figs. 4(i)–4(l). Negative β_{0w} values simply lead to a decrease of the velocity of the contact point. Positive β_{0w} values lead to an inversion of the velocity. Thus we find an increasing angular velocity with increasing β_{0w}.

B. Particle-particle collisions

The collisions of particles with each other are different from collisions with a fixed boundary. In Fig. 5 we plot snapshots from three simulations of ten pairs of colliding particles, four pictures of each simulation, and a time of 4 ms between two pictures. The initial velocities are $v_x = \pm 0.5$ m/s, $v_y = 0$ m/s, and $\omega = 0$. We vary the ratio of tangential and normal velocity by moving the right particle of each pair a distance b_0 upwards. From bottom to top $b_0 = 0, 0.1d,...,$ and $0.9d$. We use the coefficient of normal restitution $\epsilon = 0.9$ and the coefficient of maximum tangential restitution $\beta_0 = 0.5$ and vary the coefficient of friction $\mu = 0.0$ [5(a)–5(d)], $\mu = 0.2$ [5(e)–5(h)], and $\mu = 0.5$ [5(i)–5(l)]. These values of μ lead to $-\tan\gamma_0 = 0$, 0.89, and 1.33. The total linear momentum is conserved for each collision, but the relative momentum may be transferred from one direction to a perpendicular one, if the collision parameter, b_0, increases [for example, compare Figs. 5(b) and 5(c), the third pair from the top]. In these simulations, the values $b_0 = 0, 0.1d,..., 0.9d$, correspond to $\Psi_1 = 0$, 0.1005, 0.204, 0.314,..., 1.333, and 2.065, respectively. If μ is larger than zero, a transfer of linear to angular momentum takes place, see Figs. 5(e)–5(l). For small Ψ_1 values, i.e., small b_0 values, the tangential velocities are small

and therefore, the angular momentum after the collision is small too. With increasing Ψ_1 the angular momentum after collision increases, until it is limited by Coulomb's law in the range of $\Psi_1 > -\tan\gamma_0$.

The coefficient of normal restitution is material and, possibly, velocity dependent. For the sake of simplicity we do not introduce any velocity dependence of ϵ here. In order to get an idea of the consequences of different ϵ values for particle-particle collisions we plot several simulations with varying ϵ in Fig. 6. We use the same initial conditions, as for Fig. 5, with $\mu = 0.2$ and $\beta_0 = 0.5$. We compare rather inelastic collisions, $\epsilon = 0.2$ [6(a)–6(d)], with collisions of particles made of aluminum, $\epsilon = 0.6$ [6(e)–6(h)], and with almost elastic contacts, $\epsilon = 0.99$ [6(i)–6(l)]. For small b_0, we find a strong dependence of the normal velocity after contact on the value of ϵ, i.e., a lot of relative momentum is lost for small ϵ. For large b_0, the results depend much less on ϵ. In the intermediate b_0 regime, larger rotational velocities occur for larger ϵ values.

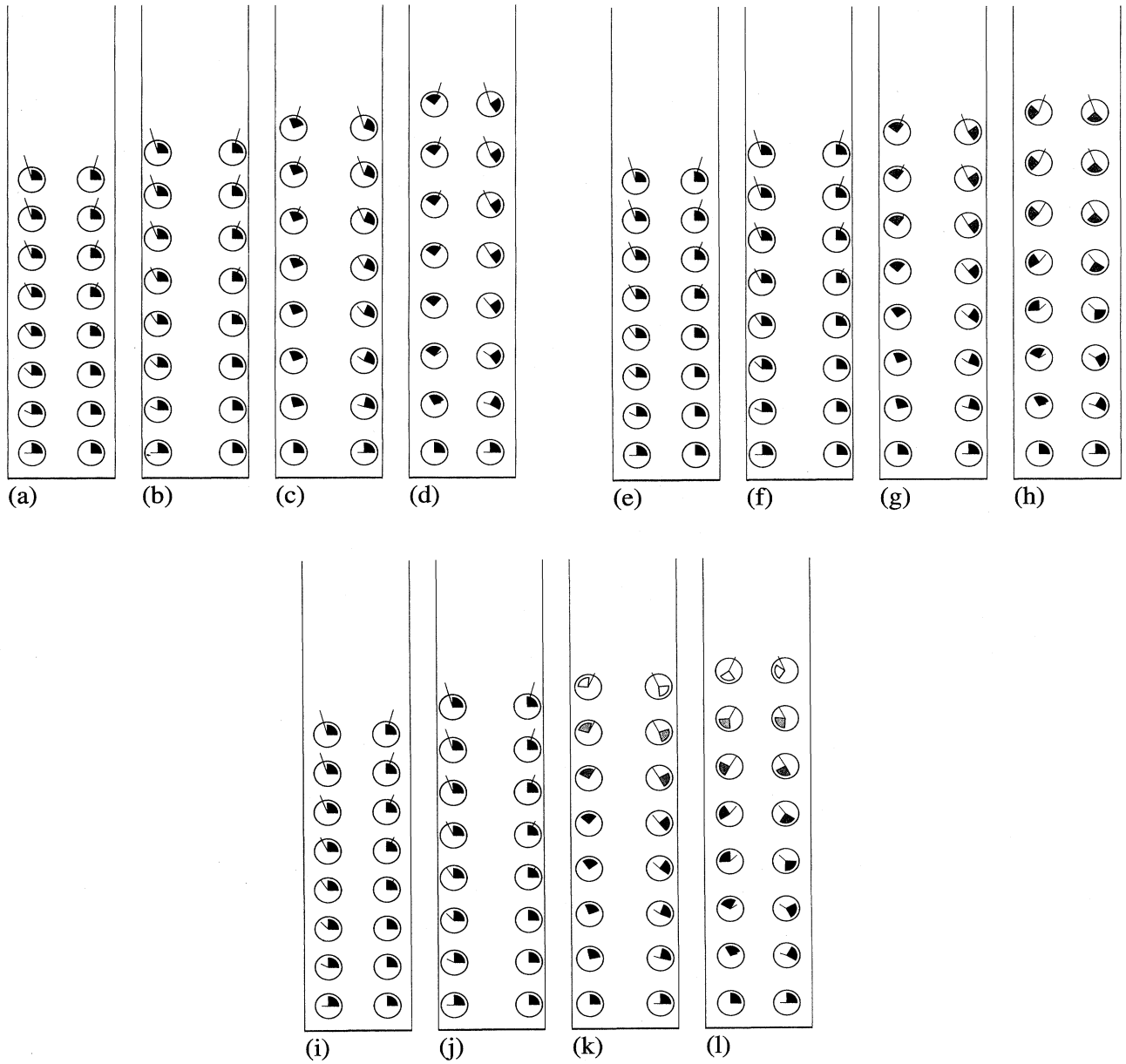

FIG. 3. Snapshots of particle wall collisions with $v_0^{(n)} = 0.5$ m/s, and $v_0^{(t)} = 0.0, 0.25, \ldots, 1.75$ m/s from bottom to top. The velocities are indicated by the lines. The angular velocity, ω, initially equals zero and is indicated by the greyscale of the quarter circles. The parameters are $\epsilon_w = 0.9$, $\beta_{0w} = 0.5$, and $\mu_w = 0.2$ (a)–(d), 0.5 (e)–(h), 10^4 (i)–(l).

C. Consequences

In this section we present some examples of particle-wall and particle-particle collisions with different coefficients of restitution and friction. We observe an interesting behavior when varying either the ratio of tangential and normal velocity, Ψ_1, or the parameters ϵ, μ, and β_0. With the model we use, it is possible to classify pair collisions, i.e., particle-particle or particle-wall collisions in terms of Ψ_1 and Ψ_2. However, the behavior of a system of many particles in a vibrating box is still to be examined. For many particle systems, the ratio of tangential and normal velocity, Ψ_1, is different for each collision. Therefore, we will perform several simulations of vibrated granular media in 2D, in order to understand the more complex, many particle systems.

V. RESULTS AND DISCUSSION

We study the behavior of N particles of diameter d_i ($i = 1, ..., N$), randomly chosen from the interval $[d_0 - w_0,$

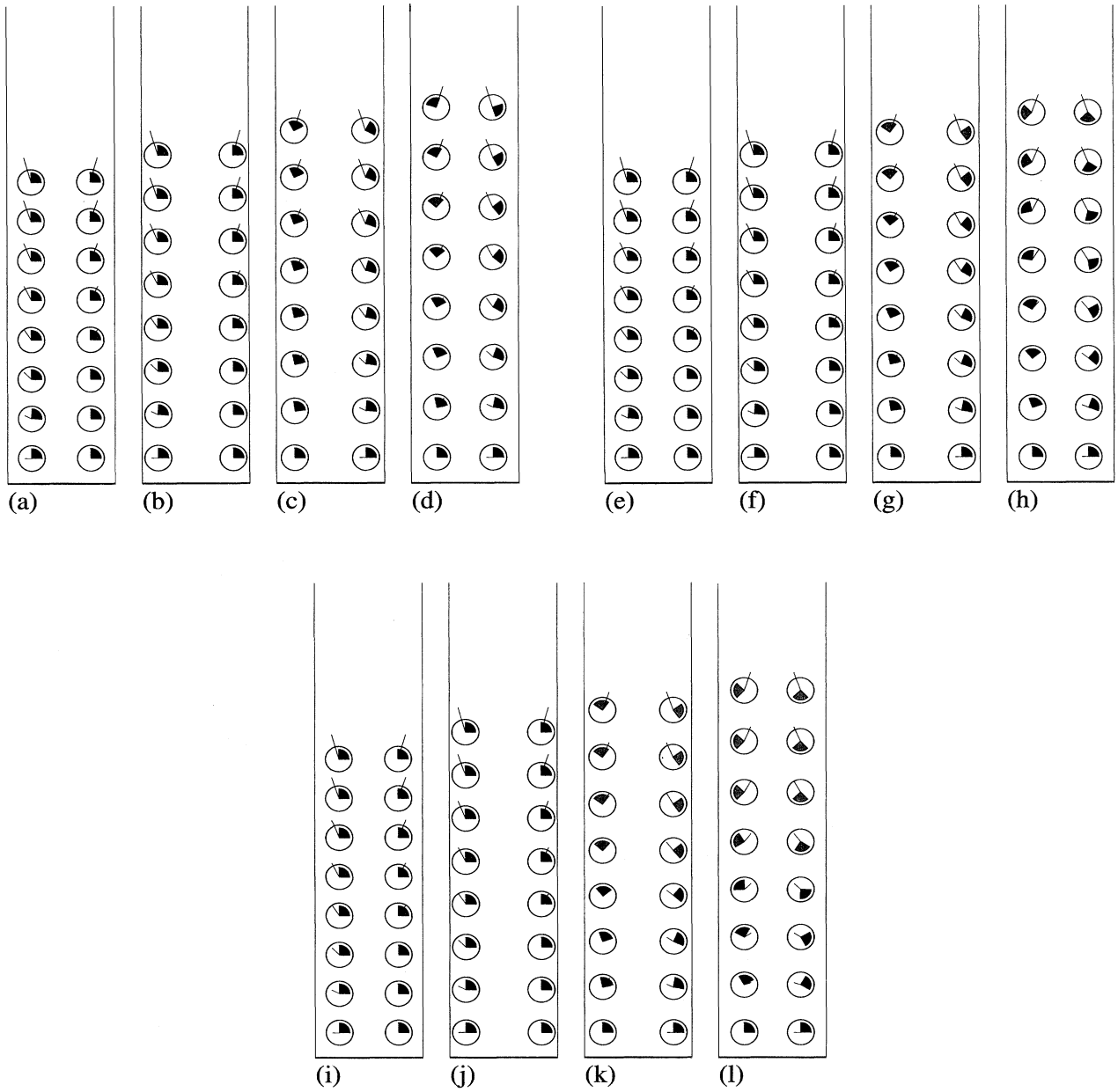

FIG. 4. Snapshots of simulations, with the same initial conditions as in Fig. 3. Here $\beta_{0w} = -0.5$ (a)–(d), $\beta_{0w} = 0.0$ (e)–(h), and $\beta_{0w} = 0.5$ (i)–(l), $\epsilon_w = 0.9$, and $\mu_w = 0.5$.

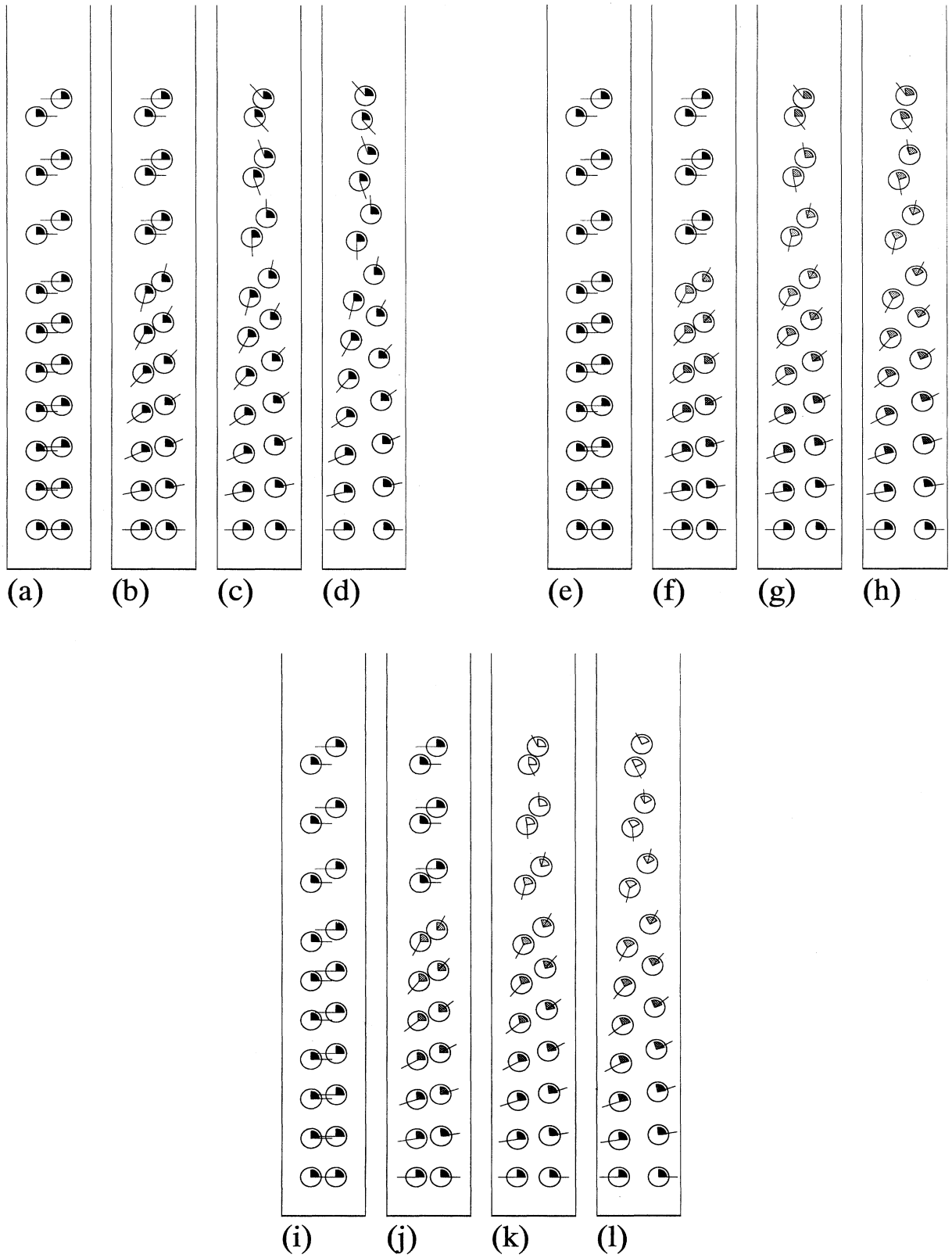

FIG. 5. Snapshots from simulations with ten pairs of particles each. Here $v_x = \pm 0.5$ m/s, $v_y = 0$ m/s, and $\omega = 0$. From bottom to top, the collision parameter is $b_0 = 0, 0.1d, \ldots, 0.9d$. The coefficient of normal restitution is $\epsilon = 0.9$ and the coefficient of tangential restitution is $\beta = 0.5$. We use different coefficients of friction, i.e., $\mu = 0.0$ (a)–(d), $\mu = 0.2$ (e)–(h), and $\mu = 0.5$ (i)–(l).

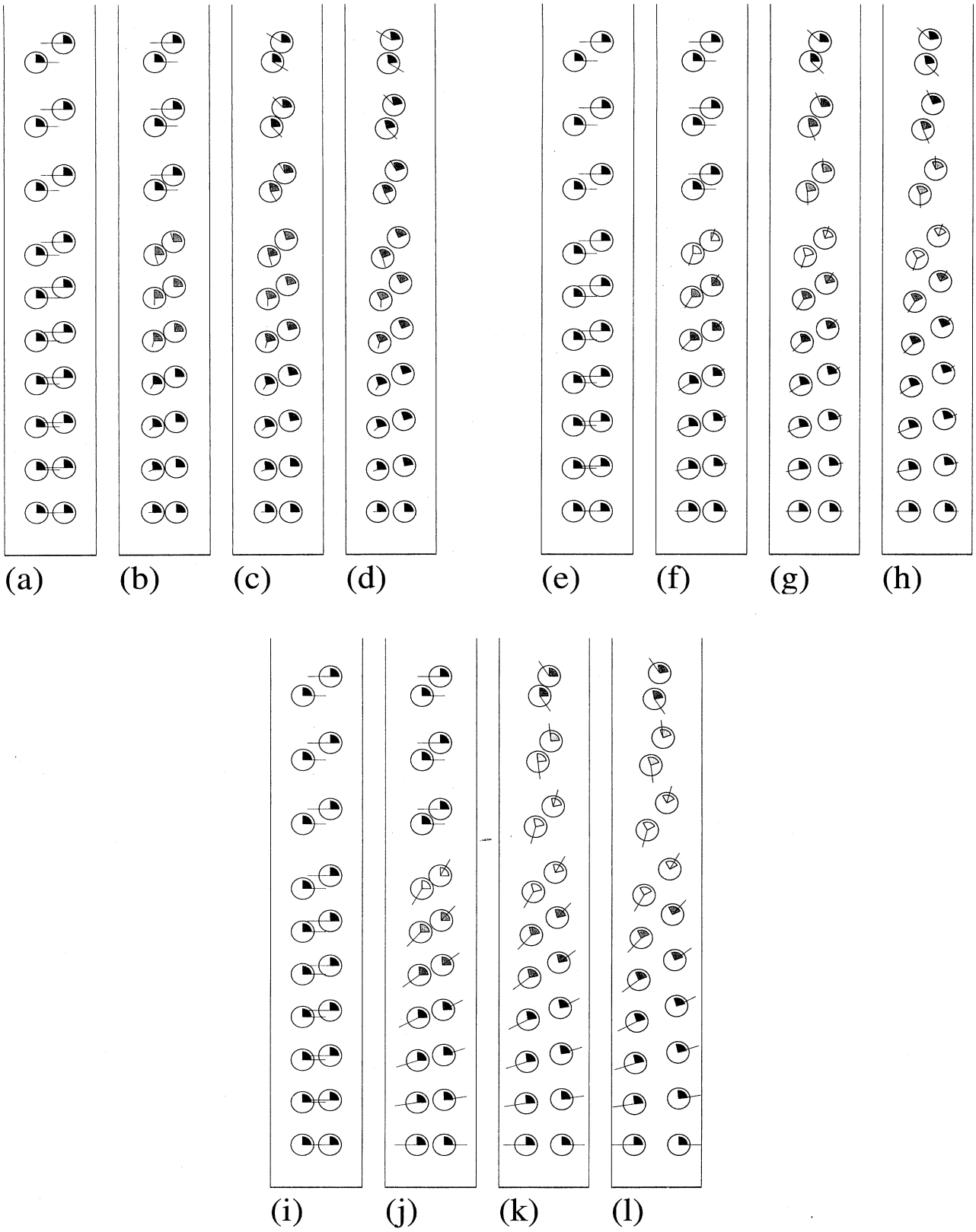

FIG. 6. Snapshots from three simulations, with the same initial conditions as in Fig. 5. Here, we vary $\epsilon = 0.2$ (a)–(d), $\epsilon = 0.6$ (e)–(h), and $\epsilon = 0.99$ (i)–(l), while $\beta = 0.5$ and $\mu = 0.2$.

$d_0 + w_0$]. If not mentioned explicitly, $d_0 = 1$ mm and $w_0 = 0.1$ mm. The properties of these particles are defined through the coefficient of normal restitution ϵ, the coefficient of friction μ, and the coefficient of maximum tangential restitution β_0. We put the particles into a container of width L and infinite height. As a simplification, we assume for most of our simulations that the bottom of the container is elastic and perfectly smooth, i.e., $\epsilon_b = 1$ and $\mu_b = 0$. At first, we concentrate on particles with a rough surface and neglect friction with the side-walls of the container, i.e., $\epsilon_w = 1$ and $\mu_w = 0$. Later, we will also examine the effect of rough walls.

In the following, we calculate three different average quantities of the system: the reduced height of the center of mass H, the kinetic energy K, and the rotational energy R. We perform the averages at phase zero, i.e., when the bottom moves upwards with velocity $V = A_0\omega$.

We calculate the reduced height of the center of mass, $H = h_{\text{c.m.}} - h_{\text{c.m.0}}$, with the height of the center of mass, $h_{\text{c.m.}} = (1/M)\sum_{i=1}^{N} m_i z_i$. M is the total mass of the particles, $M = \sum_{i=1}^{N} m_i$, with the mass m_i and the vertical coordinate z_i of particle i. The average mass of one particle is $m = M/N$, and the height of the center of mass at rest is

$$h_{\text{c.m.0}} = \frac{n_b d_0}{2N}\left[(1-\sqrt{3}/2)n_h + \sqrt{3}/2n_h^2\right] + \frac{n_o d_0}{2N}\left[1+\sqrt{3}n_h\right]. \quad (14)$$

Here n_b is the average number of beads per layer in the presence of walls, $n_h = \text{int}[N/n_b]$ is the number of full layers, and $n_o = N - n_h n_b$ is the number of beads in the uppermost layer. Note that Eq. (14) is exact in the case of monodisperse particles only. As an example, for $N = 50$ and $L = 10d_0$ we approximate $n_b \approx 9$, since due to the size fluctuations of the particles, we almost always find nine particles per layer, but not ten, as would ideally fit into the box. Thus we use for $N = 50$ and $L/d_0 = 10$ the values $n_b = 9$, $n_h = 5$, and $n_o = 5$, which leads to $h_{\text{c.m.0}} = 2.492 \times 10^{-3}$ m. Varying n_b by ± 1 we tested that H does not depend on the specific value of n_b for velocities $V > 0.1$ m/s. For larger amplitudes, i.e., lower frequencies as used in this study additional tests have to be performed, in order to verify Eq. (14) for particles of different size.

The average potential energy per particle is mgH, with $g = 9.81$ m/s^2 being the gravitational acceleration. Apart from the constant prefactor $m/2$, the average kinetic energy per particle is $K = (1/M)\sum_{i=1}^{N} m_i v_i^2$, with v_i being the velocity of particle i. In analogy, we define the rotational energy as $R = (q/M)\sum_{i=1}^{N} m_i(\frac{d_i}{2}\omega_i)^2$, with ω_i being the angular velocity of particle i. For more details on q, the factor describing the structure of the particles, see Appendix A.

A. Simulations with elastic walls

At first, we examine the behavior of the system when the coefficient of friction changes. Using $N = 50$, $\epsilon = 0.9$, $\beta_0 = 0.5$, and elastic, smooth walls, we vary the coefficient of friction μ from 0 to 20. The two limits correspond to no friction and to an almost perfectly rough surface respectively. In Fig. 7(a) we plot the reduced height of the center of mass H versus μ for two values of V, i.e., $V = 1.57$ m/s and $V = 0.314$ m/s. For $V = 0.314$ m/s we vary the frequency f, such that $f = 40$, 100, and 500 Hz, and for $V = 1.57$ m/s we use $f = 100$ Hz. The standard deviation of the H values lies between 10% and 15% of the absolute value of H. We find that H depends slightly

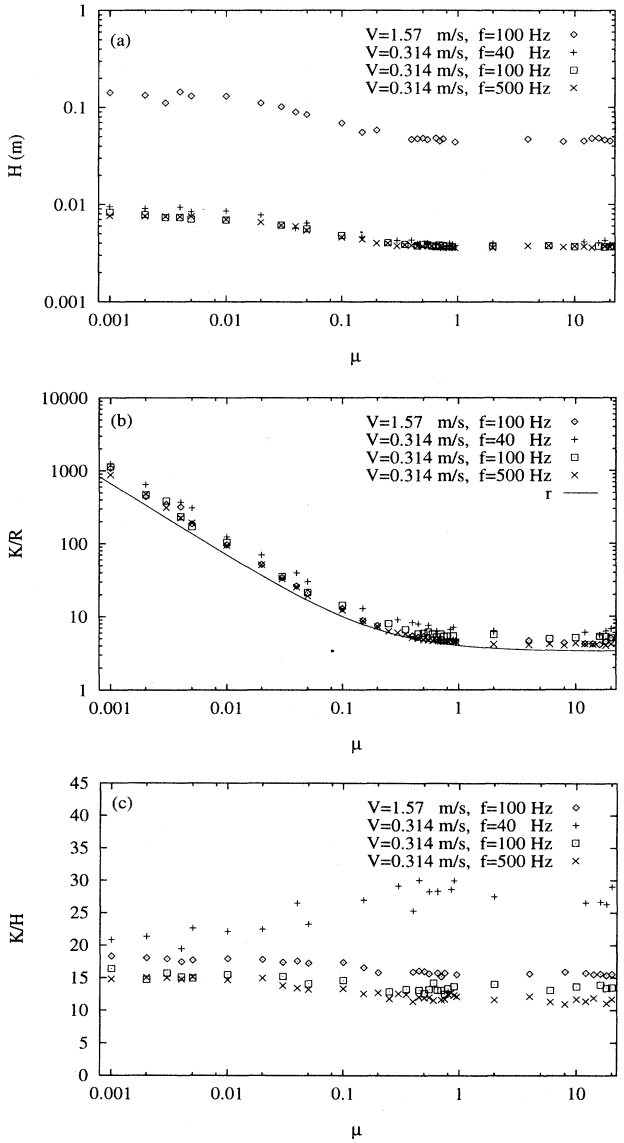

FIG. 7. (a) The reduced height of the center of mass, H, is plotted vs μ in log-log scale. The parameters are $N = 50$, $n_b = 10$, $\epsilon = 0.9$, and $\beta_0 = 0.5$. The values of the typical velocity, V, and of the frequency, f, can be extracted from the insert. (b) The ratio of kinetic and rotational energy, K/R, is plotted vs μ in log-log scale. The simulations are the same as in (a) and the line represents Eq. (15). (c) The ratio of kinetic energy and reduced height, K/H, is plotted vs μ in lin-log scale. The simulations are the same as in (a).

on μ, i.e., for increasing μ the potential energy decreases. Note that the value of H does not change, as long as V stays constant. This fact is consistent with the scaling laws found in Refs. [16,19]. Furthermore, H saturates in both limits $\mu \ll 1$ and $\mu \gg 1$. H for a perfectly smooth surface is approximately two times larger than H for a completely rough surface. In Fig. 7(b) we plot the ratio of kinetic energy and rotational energy for the same simulations, as presented in Fig. 7(a). We observe that the data coincide even for different V values. The ratio K/R seems to be rather independent of the external parameters A_0 and ω. However, there exists a dependence of K/R on the coefficient of friction μ. The line in Fig. 7(b) is the function

$$r = \frac{(2/q) + (1/\mu)}{(1+\beta_0)}, \tag{15}$$

with $q = 2/5$ and $\beta_0 = 0.5$. q determines the moment of inertia of the particles and is discussed in Appendix A. We get r, the effective coupling between kinetic and rotational energy, from the following assumptions for the limiting regimes. For weak coupling, i.e., small μ, the rotational degree of freedom is weakly excited and we expect $r \propto 1/\mu$. For strong coupling r should not depend on μ. In this regime, the kinetic and angular velocities are of the same order of magnitude, i.e., $v_{x0}^2 \approx v_{z0}^2 \approx (d\omega_{y0}/2)^2 \approx v_0^2$. Here the indices x, z, and y correspond to the directions horizontal, vertical, and perpendicular to the plane of motion, respectively. We have two linear and one rotational degrees of freedom, and with $K \approx v_{x0}^2 + v_{z0}^2$ and $R \approx q(\omega_{y0} d/2)^2$, we get $r \propto 2/q$. We find that r diverges, for vanishing μ or q. For vanishing $(1+\beta_0)$ we expect $r \propto (1+\beta_0)^{-1}$, since $\beta_0 = -1$ corresponds to a smooth surface. For small $(1+\beta_0)$ we find almost all collisions in the regime of broken contacts, such that Eq. (12) determines the velocity after contact. For large values of $(1+\beta_0)$ only a certain partition of the collisions is governed by Eq. (12), the rest follows Eq. (11), independently of β_0. Thus, if $(1+\beta_0)$ is small, it affects the rotational velocities after contact strongly. If $(1+\beta_0)$ is large, the effect is rather weak. Therefore, we assume the multiplicative factor $(1+\beta_0)^{-1}$ in Eq. (15). In Fig. 7(c) we plot the ratio of K and H, i.e., K/H versus μ for the same simulations, as presented in Fig. 7(a). Equipartition of potential and kinetic energy, i.e., $mgH = (m/2)K$, here corresponds to a ratio $K/H = 2g$. We find that the ratio of kinetic and potential energy is smaller than expected, except for the low frequency data (crosses). Also, except for low frequencies, the ratio K/H decreases slightly with increasing μ.

Now we are interested in how far β_0 affects the behavior of the vibrated system. Therefore we use the same parameters as for Fig. 7, i.e., $N = 50$, $\epsilon = 0.9$, and two different values for the velocity: $V = 1.57$ m/s and $V = 0.314$ m/s with $f = 100$ Hz. Here, we fix $\mu = 0.2$ and vary β_0 from -1 to 1. $\beta_0 = -1$ corresponds to no friction, whereas $\beta_0 = 1$ corresponds to a complete inversion of the tangential velocity for small values of Ψ_1. For small Ψ_1, the tangential velocity before contact is small compared to the normal velocity. In Fig. 8(a) we plot the reduced height of the center of mass H versus β_0. We find that H is almost constant for $\beta_0 > -0.5$; for smaller β_0, H increases, since rotation of particles becomes less and less important. In order to display the strength of rotation, we plot in Fig. 8(b) the ratio K/R as a function of β_0. We find that the ratio K/R diverges for decreasing β_0. The line in Fig. 8(b) represents Eq. (15) with $q = 2/5$ and $\mu = 0.2$. The ratio K/H is, besides a slight decrease with increasing β_0, almost independent of β_0, as can be seen from Fig. 8(c).

The third parameter that influences the rotational en-

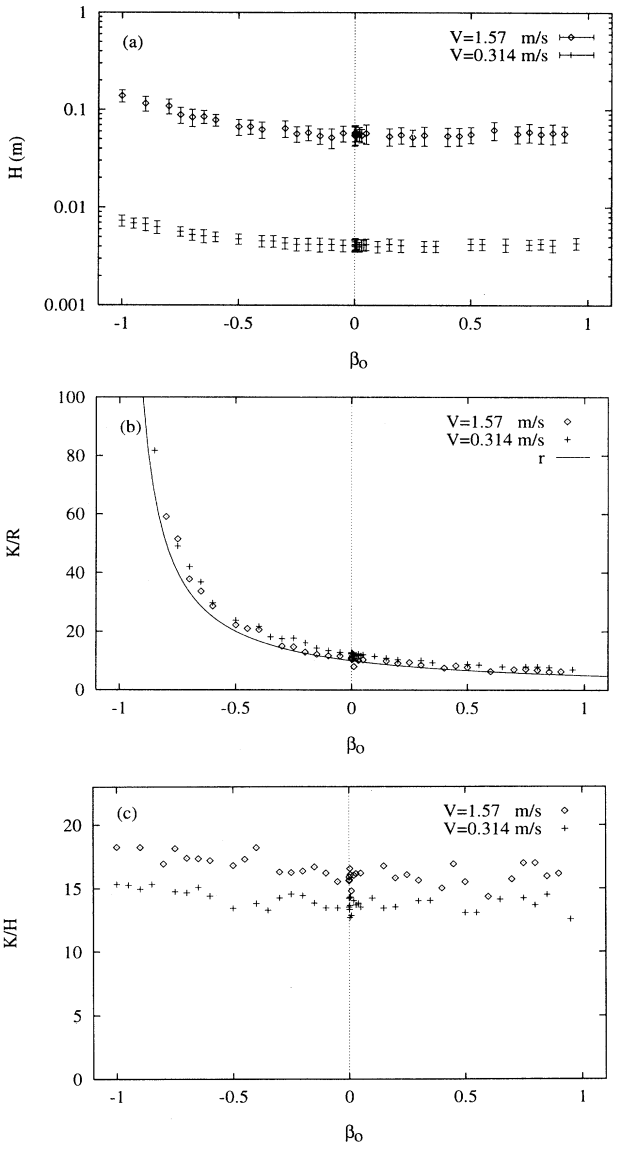

FIG. 8. (a) The reduced height of the center of mass, H, is plotted vs β_0 in log-lin scale. The parameters are $N = 50$, $n_b = 10$, $\epsilon = 0.9$, $\mu = 0.2$. $f = 100$ Hz and the values of the typical velocity, V, can be extracted from the insert. (b) The ratio of kinetic and rotational energy, K/R, is plotted vs β_0 for the same simulations as in (a). The line represents Eq. (15). (c) The ratio of kinetic energy and reduced height, K/H, is plotted vs β_0. The simulations are the same as in (a).

ergy R of the system is the moment of inertia $I = qm(d/2)^2$ of the particles used. To demonstrate the importance of this quantity, we use the same parameters as before in Fig. 8, i.e., $N = 50$, $\epsilon = 0.9$, and two different values for the velocity: $V = 1.57$ m/s and $V = 0.314$ m/s, with $f = 100$ Hz. We use different μ values, $\beta_0 = 0$, and vary q from 0 to 1. The lower and upper limits correspond to particles with all their mass at the center or to rings, i.e., 2D particles with all their mass, a distance $d/2$ away from the center. The dependence of H on q is plotted in Fig. 9(a). The qualitative behavior of the center of mass is the same as in Figs. 7 and 8. H decreases with increasing q, i.e., with rotational energy getting larger and larger. However, we find no dependence of H on q for experimentally relevant situations with either spheres, i.e., $q = 2/5$, or disks, i.e., $q = 1/2$. From Fig. 9(b), where K/R is plotted versus q, we infer that q is a parameter like μ or β_0, i.e., a measure for the ratio K/R. The line in Fig. 9(b) gives Eq. (15) with $\mu = 0.25$ and $\beta_0 = 0$. In Fig. 9(c) we plot K/H versus q and find this ratio only slightly decreasing with increasing q.

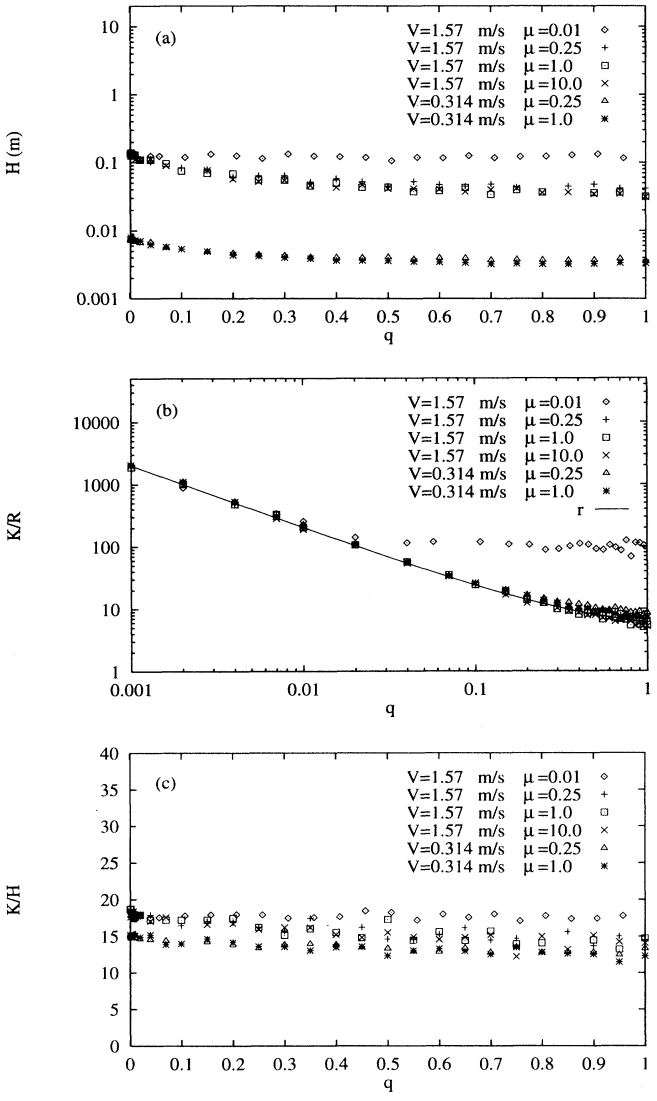

FIG. 9. (a) The reduced height of the center of mass, H, is plotted vs q in log-lin scale. The parameters are $N = 50$, $n_b = 10$, $\epsilon = 0.9$, and $\beta_0 = 0$. $f = 100$ Hz and the values of the typical velocity, V, and of the coefficient of friction, μ, can be extracted from the insert. (b) The ratio of kinetic and rotational energy, K/R, is plotted vs q in log-log scale. The simulations are the same as in (a). The line represents Eq. (15) with $\mu = 0.25$. (c) The ratio of kinetic energy and reduced height, K/H, is plotted vs q for the same simulations as in (a).

We remark that the limits of $\mu = 0$, $\beta_0 = -1$, and $q = 0$ in Figs. 7(a), 8(a), and 9(a) coincide because all these limits correspond to the case of no rotation. For the same reason, the ratio K/R diverges in Figs. 7(b), 8(b), and 9(b) on the left-hand sides of the plots, when the variables approach the above limits. Note that the phenomenological function r, see Eq. (15), is systematically too small to fit K/R in Figs. 7(b) and 8(b). A factor of 1.3 ± 0.2 in Eq. (15) leads to a better agreement between numerical simulations and phenomenological function r. The above simulations show that kinetic and potential energy are of the same order of magnitude, i.e., the ratio K/H depends only slightly on the frictional parameters. In contrast, the rotational energy is coupled with the kinetic energy via $R \propto K/r$, with r being a function of the parameters μ, β_0, and q.

B. Simulations with rough, dissipative walls

In Ref. [19] an interesting behavior of the reduced height of the center of mass H on the typical velocity V was observed in computer simulations. It is documented that

$$H \propto V^{\delta}, \tag{16}$$

with $\delta = 1.5$ in 2D. The simulations were performed for smooth particles, i.e., neglecting rotation and preferentially use a box with smooth but dissipative walls, i.e., $\epsilon_w < 1$.

Experiments were performed with the same model system, but with rough particles [16,21]. The experiments confirm the scaling law $H \propto V^{\delta}$, with a somewhat smaller δ between $\delta = 1.3$ and $\delta = 1.4$. However, taking into account the fluctuations of the quantity H and the different boundary conditions, this agreement is still satisfactory. Also the experiments were performed in the small velocity range 0.1 m/s $< V <$ 1 m/s, whereas the simulations explore the range 0.1 m/s $< V <$ 10 m/s.

At first we test which influence the rotation of particles has on H when we vary V. Therefore, we simulate $N = 50$ particles in a box of width $L/d_0 = 10$ with elastic, $\epsilon_w = 1$, and smooth, $\mu_w = 0$, walls. In Fig. 10, we plot H as a function of V for either smooth, $\mu = 0$, label (1), or rough, $\mu = 0.2$ and $\beta_0 = 0.5$, label (2), particle surface. In order to check if the results are affected by the size of the container, we perform additional simulations with $\mu = 0.2$, and $\beta_0 = 0.5$, using $N = 150$, $L/d_0 = 30$, label (3), and $N = 250$, $L/d_0 = 50$, label (4). From Fig. 10 we

find that friction between particles leads to a systematic reduction of H for given V, compare Fig. 7(a). Furthermore, we observe no dependence of H on the system size, as long as the ratio N/L is constant. Different from the scaling laws predicted by simulations [19] and experiments [16], we observe in the case of elastic, smooth walls a large value of $\delta \approx 2$ for $V > 1$ m/s. Note that for such large values of V, the system is dilute. The experiments were carried out in the range $V < 1$ m/s and therefore could not observe this behavior. The simulations used smooth, but dissipative walls in the range $V > 1$ m/s, where $\delta \approx 3/2$ was observed. Thus the properties of the walls affect δ in the dilute case.

Now, we compare systems with different walls, either smooth and elastic, smooth and dissipative, or rough and dissipative. In Fig. 11 we plot H as a function of V for $N = 50$, $\epsilon = 0.9$, $\mu = 0.2$, $\beta_0 = 0.5$, and $L/d_0 = 10$. We compare simulations with elastic, $\epsilon_w = 1$, and perfectly smooth, $\mu_w = 0$, walls, see label (1), with simulations, using dissipative walls, $\epsilon_w = 0.9$, see labels (2) and (3). We have either smooth, $\mu_w = 0$, label (2), or rough walls, $\mu_w = 0.2$, $\beta_{0w} = 0.5$, label (3). Note that distinct from Ref. [19], rotation of the particles is allowed, and particle-particle contacts include friction. We observe in the case of dissipative, smooth walls, i.e., label (2), that the height H behaves as predicted by Luding *et al.* [19]. The power $\delta = 3/2$ is indicated by the dotted line, label (4). For elastic, smooth walls, label (1), the power δ changes from $\delta = 3/2$, for $V < 1$ m/s, to $\delta = 2$ for $V > 1$ m/s. The crossover is marked with the arrow and the dash-dotted line, label (5), indicates the slope 2. Note that the crossover occurs not necessarily for $V = 1$ m/s; only for the simulations presented here, we find $\delta \approx 2$ for $V > 1$ m/s. In the dilute regime, collisions between particles and the walls occur more frequent and thus the walls' properties become more important. Dissipative walls, i.e., the value of ϵ_w, does not change the behavior of H, as long as particle-wall collisions are rare, i.e., $V < 1$ m/s. In contrast, the power δ depends on ϵ_w in the dilute regime, where particles preferentially collide with the walls. This behavior is connected to the

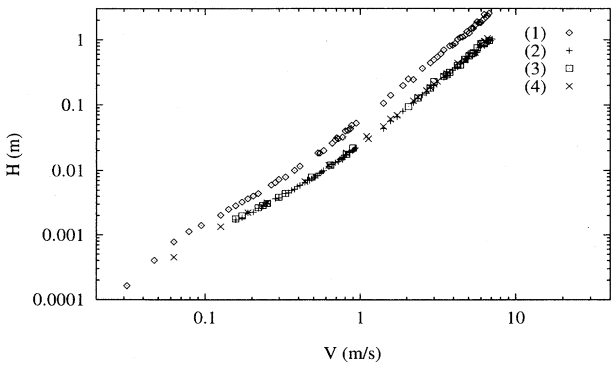

FIG. 10. Reduced height, H, vs typical velocity, V, in log-log scale. The parameters used are $\epsilon = 0.9$, $\beta_0 = 0.5$, and $\mu = 0$ for (1), or $\mu = 0.2$ for (2)–(4). Furthermore, $N = 50$ for (1), (2), $N = 150$ for (3), $N = 250$ for (4), and $L/d_0 = 10$, 30, and 50.

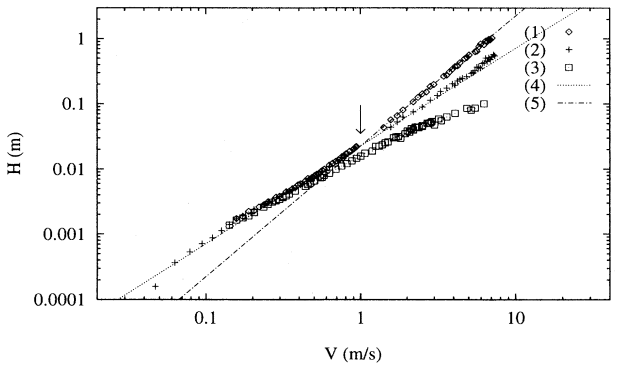

FIG. 11. H vs V in log-log scale. The parameters used are $\epsilon = 0.9$, $\mu = 0.2$, $\beta_0 = 0.5$, $N = 50$, and $L/d_0 = 10$. The properties of the walls are $\beta_{0w} = 0.5$ and different ϵ_w and μ_w, i.e., $\epsilon_w = 1$, $\mu_w = 0$ for (1), $\epsilon_w = 0.9$, $\mu_w = 0$ for (2), and $\epsilon_w = 0.9$, $\mu_w = 0.2$ for (3). The lines (4) and (5) indicate the slopes 3/2, and 2, respectively. The arrow marks the transition from power 3/2 to power 2 for the data (1). Here, the walls are fixed and only the bottom moves.

mean free path l of one particle. If $l \ll L$, the system is dense and we find $\delta \approx 3/2$, independent of ϵ_w. For $l \gg L$ we find $\delta \approx 3/2$ for dissipative walls, and $\delta \approx 2$ for elastic walls [35]. Rough walls, label (3), make the behavior even more difficult. Compared to the data for smooth walls, label (2), the height H is more and more reduced with increasing V. For large V, the value of δ is not longer constant, and also depends on μ.

One reason for this strange behavior, for rough walls, may be the boundary condition of our system. For the simulations presented in Fig. 11, we used fixed walls where only the bottom was moving. In order to check the effect of vertically moving walls we plot in Fig. 12 the results of simulations, performed using rough, but moving walls, i.e., $\mu_w = 0.2$, see label (1), and $\mu_w = 0.5$, see label (2). The vertical motion of the walls follows Eq. (13). The data labeled (3) are the same as in Fig. 11, and

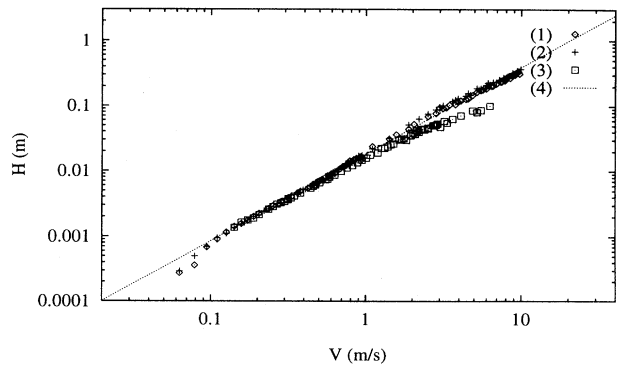

FIG. 12. H vs V in log-log scale. The parameters used are $\epsilon = 0.9$, $\mu = 0.2$, $\beta_0 = 0.5$, $N = 50$, and $L/d_0 = 10$. The properties of the walls are $\beta_{0w} = 0.5$, $\epsilon_w = 0.9$, and different μ_w, i.e., $\mu_w = 0.2$ for (1,3), and $\mu_w = 0.5$ for (2). For the simulations (1,2) the walls move according to Eq. (13), and the data (3) correspond to data (3) of Fig. 11, i.e., fixed walls. The line (4) indicates the best fit to the data (1) and (2) for $V > 0.1$ with the slope 1.33.

the other parameters are $\epsilon = 0.9$, $\mu = 0.2$, $\beta_0 = \beta_{0w} = 0.5$, $N = 50$, and $L/d_0 = 10$, as before. A best fit of the data (1) and (2) leads to the line (4), with a slope $\delta \approx 1.33$. Thus, it is important to take care of the motion of the walls in the case of rough walls. Furthermore, $\delta = 1.33$ is in agreement with the experimental results [16].

C. Comparison with experiments

We now perform a direct comparison of our simulations with recent experiments [16]. Therefore, we duplicate the experimental setup, i.e., we use $L = 165$ mm. We set the vibration frequency to $f = 50$ Hz and use different amplitudes, $A_0 = 0.5$, 1.12, 1.84, and 2.12 mm. For each amplitude we perform simulations with different particle numbers, $N = 27$, 40, 60, and 90. We use particles of the same diameter, i.e., $d_0 = 5$ mm and $w_0 = 0$, with the coefficients of normal restitution, $\epsilon = \epsilon_w = \epsilon_b = 0.92$. The coefficients of friction are $\mu = \mu_w = \mu_b = 0.22$, and the coefficients of maximum tangential restitution are here $\beta_0 = \beta_{0w} = \beta_{0b} = 0$.

Paralleling Figs. 15 and 16 of Ref. [16], we plot $H = h_{\mathrm{c.m.}} - h_{\mathrm{c.m.0}}$ as a function of $V = A_0\omega$ in Fig. 13(a) and as a function of the inverse number of layers, $h = n_b/N$ in Fig. 13(b). The simulations are not in perfect agreement with the experimental data. To compare the simulations with the experiments, we perform power law fits of the form $H \propto V^{\delta}$. The experiments lead to $\delta = 1.239$, 1.310, 1.326, and 1.022 for $N = 27$, 40, 60, and 90, respectively, whereas best fits to our data result in $\delta = 1.72$, 1.66, 1.57, and 1.45. From these δ values we calculate $\overline{\delta} = 1.60 \pm 0.10$. Figure 13(b) shows that also the dependence of H on the number of particles N is different in simulations and experiments. Power law fits of the form $H \propto (n_b/N)^{\nu}$ to the experimental data lead to $\nu = 0.140$, 0.172, 0.396, and 0.350 for $f = 50$ Hz and amplitudes $A_0 = 0.5$, 1.12, 1.84, and 2.12 mm, respectively. Fits to the simulations lead to $\nu = 0.60$, 0.71, 0.81, and 0.91 such that $\overline{\nu} = 0.76 \pm 0.11$. These simulations were performed with a container of infinite height. Simulations in a container with height 285 mm lead to the averaged powers $\overline{\delta} = 1.52 \pm 0.06$ and $\overline{\nu} = 0.70 \pm 0.08$. These powers are still systematically larger than the experimentally observed ones. The reduced slopes come from the simulations with large amplitude and small numbers of particles in which sometimes a particle hits the top.

One reason for such large exponents of δ and ν is possibly the value of ϵ_b. Therefore, we perform the same simulations as for Fig. 13, only using different values for the restitution with the bottom, i.e., $\epsilon_b = 0.84$ and 0.96. For decreasing ϵ_b, we observe a decreasing H, but we do not observe a significant dependence of δ on ϵ_b. Also ν decreases only slightly with decreasing ϵ_b.

Another possible reason for the discrepancy between experiment and simulation is the experimental setup which is not really two-dimensional, i.e., particles may collide with front and back walls. The simulations of the preceding subsection have shown that dissipative, rough sidewalls in a 2D setup possibly change the exponent δ. Thus, we expect that front and rear walls in the third dimension also will affect the behavior of the system. In Ref. [16] an estimation of the energy loss at front and rear is presented. The estimated frictional energy loss, due to wall friction between two particle-particle contacts, was of the order of a few percent of the energy lost per particle-particle collision. Thus, further, more detailed comparisons of experiment and simulations are necessary to understand the effects which cause the differences.

VI. SUMMARY AND CONCLUSION

Following recent publications, we modeled two-dimensional systems of spheres, situated in a vibrating box. We used a collision model with experimental background and extended the model to be able to handle particles of different structure. To clarify the elementary processes, i.e., particle-wall or particle-particle collision, we presented several examples with different initial conditions and particles' properties. We checked in how far friction or particle structure changes the typical quantities of the system. Furthermore, we tested the importance of the walls for the systems' properties and compared our simulations with recent experiments.

Introducing friction between particles leads to rotational motion of the particles. Comparing the potential, the kinetic, and the rotational energies we find that po-

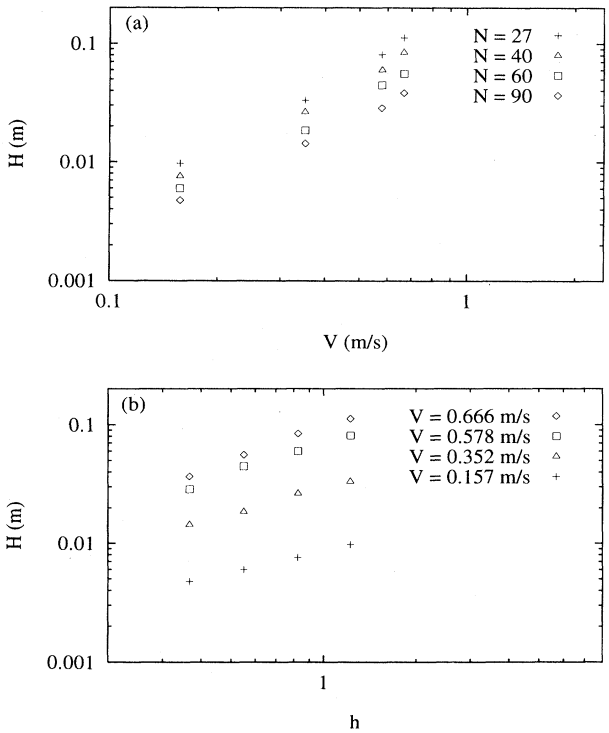

FIG. 13. (a) H vs V in log-log scale. The parameters of dissipation are $\epsilon = \epsilon_w = \epsilon_b = 0.92$, $\mu = \mu_w = \mu_b = 0.22$, and $\beta_0 = \beta_{0w} = \beta_{0b} = 0.0$. Crosses, triangles, squares, and diamonds correspond to $N = 27$, 40, 60, and 90, respectively. (b) H vs $h = n_b/N$ in log-log scale for the same simulations as in (a). Crosses, triangles, squares, and diamonds correspond to $A_0 = 0.5$, 1.12, 1.84, and 2.12 mm, respectively.

tential and kinetic energy are of the same order of magnitude, almost independent of the frictional properties of the particles. Kinetic and rotational energy are coupled via the relative velocity of the surfaces and the effective coupling parameter that relates K and R. With increasing friction, i.e., increasing roughness of the surfaces, the ratio K/R decreases until it saturates as a function of the structure of the particles, see Eq. (15).

Rough particle surfaces lead to a systematic reduction of the potential energy of the system without changing the qualitative behavior. We relate the reduction of potential energy to the additional degree of freedom, i.e., rotation. Due to rough surfaces a certain amount of kinetic energy is stored in rotational motion. This energy is not accessible for linear motion in the direction opposite to the gravitational force. Thus, both kinetic and potential energy are reduced if rough particles are used.

Interestingly, the properties of the walls affect the system in a more complicated way. In the dilute regime smooth, elastic or smooth, dissipative walls correspond to $\delta \approx 2$ or $\delta \approx 3/2$ respectively. Collisions between particles and walls occur frequently if the mean free path is comparable or larger than the system width L. Thus, the effect is stronger for less dense systems, i.e., larger H. Rough walls lead to a further reduction of the height H, because large tangential velocities relative to the walls mean strong dissipation due to friction. Overall dissipation thus depends on the frictional parameters and also on the density of the system. If we perform simulations in a container with moving, rough walls, we observe a behavior that is similar to the behavior of a system with smooth walls. Moving, rough walls lead to energy dissipation due to friction like fixed, rough walls. But sometimes, due to the velocity of the wall, energy may be input into the system. However, a system with roughness and normal dissipation, for both particles and walls, follows Eq. (16) with $\delta \approx 1.33$ over two orders of magnitude in V. This result is consistent with the experimental findings of Ref. [16].

Performing simulations with rotating particles, and relating the simulations to recent experiments, we found the height of the center of mass to be of the same order of magnitude. Note that the powers δ and ν are systematically larger in simulations, indicating problems with the three-dimensional (3D) nature of the experimental setup. The simulations we compared with the experiments were performed in a small range of V and (n_b/N) values. From other simulations, see Fig. 12, we also get the scaling law Eq. (16) with a power smaller than 2, i.e., $\delta \approx 1.33$. Recent theoretical approaches [16,22] always lead to the power $\delta = 2$. Precise comparisons of simulations, experiments, and theories are necessary to learn where the differences become eminent.

We did not examine convection in vibrated granular media, but we expect that the frictional properties of both particles and walls will play an important role for this effect. Another problem still open is the behavior of a vibrated system in 3D with respect to the power law Eq. (16). It would be of interest to know how the system behaves in 3D, and if the strange power law found in 2D, i.e. $H \propto V^{\delta}$, with $\delta < 2$, still holds in 3D.

ACKNOWLEDGMENTS

We thank J. Lee, S. Dippel, and S. Schwarzer and the granular materials group of the L.A.O.M.C. for helpful discussions and comments. Furthermore, we gratefully acknowledge the support of the European Community (Human Capital and Mobility) and of the PROCOPE scientific collaboration program.

APPENDIX A

The momentum change $\Delta\vec{P}$ is given in Eq. (10). Here, we calculate the tangential restitution, β_1, that connects Eqs. (9) and (10). Paralleling Eq. (2) the velocity of the contact point after collision is

$$\vec{u}_c = \vec{u}_1 - \vec{u}_2 - \left(\frac{d_1}{2}\vec{\omega}_1' + \frac{d_2}{2}\vec{\omega}_2'\right) \times \vec{n}. \tag{A1}$$

Inserting Eqs. (5) into Eq. (A1) and applying Eq. (2) we get

$$\vec{u}_c = \vec{v}_c + \Delta\vec{P}\frac{1}{m_{12}} + \Delta\vec{P}^{(t)}\left(\frac{d_1^2}{4I_1} + \frac{d_2^2}{4I_2}\right), \tag{A2}$$

where $I_i = q_i m_i (d_i/2)^2$ is the moment of inertia about the center of particle i. q_i depends on the structure of the particles. For example, $q = 2/5$ for a solid sphere in 3D, and $q = 1/2$ in the case of a solid disk, or $q = 1$ for a thin ring, in 2D. Inserting Eq. (9) into Eq. (A2) we get

$$\begin{aligned}\vec{u}_c &= -\epsilon\vec{v}_c^{(n)} + \left(1 + \mu(1+\epsilon)\cot\gamma(1+\tfrac{1}{q})\right)\vec{v}_c^{(t)} \\ &= -\epsilon\vec{v}_c^{(n)} - \beta_1\vec{v}_c^{(t)}.\end{aligned} \tag{A3}$$

From Eq. (A3) we simply get the tangential restitution, β_1, for Coulomb type contacts as

$$\beta_1 = -1 - \mu(1+\epsilon)\cot\gamma\left(1 + \frac{1}{q}\right). \tag{A4}$$

In the case of solid spheres, with $q = 2/5$, we have $\beta_1 = -1 - (7/2)\mu(1+\epsilon)\cot\gamma$. Note that $\cot\gamma \leq 0$ for all γ, such that $-1 \leq \beta_1$. The lower limit of β_1 corresponds to no friction.

APPENDIX B

In ED simulations the contact time, t_c, of two particles is implicitly zero, such that the momentum change $\Delta\vec{P}$ describes the collision. In MD simulations, one has $t_c > 0$, and the sum of all forces, $\vec{f}$, acting on a particle is needed to calculate the momentum change of this particle:

$$\Delta\vec{P} = \int_{t=0}^{t_c} \vec{f}\, dt. \tag{B1}$$

Knowing the impact angle, γ, it is possible to use any normal force $f^{(n)}$ together with the tangential force

$$f^{(t)} = \begin{cases} \mu f^{(n)}, & \text{for } \gamma \leq \gamma_0 \\ \mu f^{(n)} \frac{\tan\gamma}{\tan\gamma_0}, & \text{for } \gamma > \gamma_0 \end{cases}, \tag{B2}$$

where γ_0 is defined in the main text. Usually, normal forces are based on Hook, Hertz, or hysteretic interaction models. The force in Eq. (B2) leads to the ratio

$$\frac{\Delta P^{(t)}}{\Delta P^{(n)}} = \mu \ \min\left[1, \frac{\tan\gamma}{\tan\gamma_0}\right], \tag{B3}$$

which is consistent with the model described in Sec. II and introduced by [26,29]. How far this choice of forces is treatable in simulations and how it is connected to standard MD methods has to be elaborated.

[1] A. Rosato, K. J. Strandburg, F. Prinz, and R. H. Swendsen, Phys. Rev. Lett. **58**, 1038 (1987); Powder Tech. **49**, 59 (1986).

[2] P. Devillard, J. Phys. (Paris) **51**, 369 (1990).

[3] R. Jullien, P. Meakin, and A. Pavlovitch, Phys. Rev. Lett. **69**, 640 (1992).

[4] J. Duran, J. Rajchenbach, and E. Clément, Phys. Rev. Lett. **70**, 2431 (1993).

[5] E. Clément, J. Duran, and J. Rajchenbach, Phys. Rev. Lett. **69**, 1189 (1992).

[6] C. Laroche, S. Douady, and S. Fauve, J. Phys. (Paris) **50**, 699 (1989).

[7] M. Faraday, Philos. Trans. R. Soc. London **52**, 299 (1831).

[8] Y.-h. Taguchi, Phys. Rev. Lett. **69**, 1371 (1992).

[9] J. A. C. Gallas, H. J. Herrmann, and S. Sokołowski, Phys. Rev. Lett. **69**, 1375 (1992).

[10] H. K. Pak and P. P. Behringer, Phys. Rev. Lett. **71**, 1832 (1993).

[11] F. Melo, P. Umbanhowar, and H. L. Swinney, Phys. Rev. Lett. **72**, 172 (1994).

[12] C.-h. Liu and S. R. Nagel, Phys. Rev. Lett. **68**, 2301 (1992).

[13] M. Leibig, Phys. Rev. E **49**, 1647 (1994).

[14] J. Duran, T. Mazozi, E. Clément, and J. Rajchenbach, Phys. Rev. E **50**, 3092 (1994).

[15] H. M. Jaeger and S. R. Nagel, Science **255**, 1523 (1992); H. M. Jaeger, J. B. Knight, C.-h. Liu, and S. R. Nagel, Mater. Res. Bull. May, 25 (1994).

[16] S. Warr, J. M. Huntley, and G. T. H. Jacques, Phys. Rev. E (to be published).

[17] E. Clément, S. Luding, A. Blumen, J. Rajchenbach, and J. Duran, Int. J. Mod. Phys. B **7**, 1807 (1993).

[18] S. Luding, E. Clément, A. Blumen, J. Rajchenbach, and J. Duran, Phys. Rev. E **49**, 1634 (1994).

[19] S. Luding, H. J. Herrmann, and A. Blumen, Phys. Rev. E **50**, 3100 (1994).

[20] R. Mazighi, B. Bernu, and F. Delyon, Phys. Rev. E **50**, 4551 (1994); B. Bernu and R. Mazighi, J. Phys. A **23**, 5745 (1990).

[21] S. Warr, G. T. H. Jacques, and J. M. Huntley, Powder Tech. **81**, 41 (1994).

[22] J. Lee, Physica A (to be published).

[23] P. K. Haff, J. Fluid Mech. **134**, 401 (1983).

[24] S. B. Savage, Adv. Appl. Mech. **24**, 289 (1984); S. B. Savage, in *Disorder and Granular Media*, edited by D. Bideau (North-Holland, Amsterdam, 1992).

[25] C. S. Campbell, Annu. Rev. Fluid Mech. **22**, 57 (1990).

[26] S. F. Foerster, M. Y. Louge, H. Chang, and K. Allia, Phys. Fluids **6**, 1108 (1994).

[27] S. Luding, E. Clément, A. Blumen, J. Rajchenbach, and J. Duran, Phys. Rev. E **50**, R1762 (1994).

[28] S. Luding, E. Clément, A. Blumen, J. Rajchenbach, and J. Duran, Phys. Rev. E **50**, 4113 (1994).

[29] O. R. Walton and R. L. Braun, J. Rheol. **30**, 949 (1986); O. R. Walton, in *Particulate Two Phase Flow*, edited by M. C. Roco (Butterworth-Heinemann, Boston, 1992).

[30] G. A. Kohring, S. Melin, H. Puhl, H. J. Tillemans, and W. Vermöhlen, Comput. Methods in Appl. Mech. and Eng. **124**, 273 (1995).

[31] M. P. Allen and D. J. Tildesley, *Computer Simulation of Liquids* (Oxford University Press, Oxford, 1987).

[32] B. D. Lubachevsky, J. Comput. Phys. **94**, 255 (1991).

[33] S. McNamara and W. R. Young, Phys. Fluids A **4**, 496 (1992); **5**, 34 (1993).

[34] Y. Du, H. Li, and L. P. Kadanoff, Phys. Rev. Lett. **74**, 1268 (1995).

[35] S. Luding, Ph.D. thesis, University of Freiburg, 1994 (unpublished).

[36] C. E. Brennen, S. Gosh, and C. Wassgren, in *Powders & Grains 93*, edited by C. Thornton (Balkema, Rotterdam, 1993).

[37] A. D. Rosato and Y. Lan, in *Powders & Grains 93*, edited by C. Thornton (Balkema, Rotterdam, 1993).

[38] N. Maw, J. R. Barber, and J. N. Fawcett, Wear **38**, 101 (1976).

[39] In Refs. [26,29], β_0 is limited to $0 \leq \beta_0 \leq 1$.